THE ASTROPHYSICAL JOURNAL LETTERS, 820:L15 (6pp), 2016 March 20 doi:10.3847/2041-8205/820/1/L15

MAGNETIC FIELD AND WIND OF KAPPA CETI: TOWARD THE PLANETARY HABITABILITY OF THE YOUNG SUN WHEN LIFE AROSE ON EARTH

J.-D. DO NASCIMENTO, JR.[1,2], A. A. VIDOTTO[3,13], P. PETIT[4,5], C. FOLSOM[6], M. CASTRO[2], S. C. MARSDEN[7], J. MORIN[8], G. F. PORTO DE MELLO[9], S. MEIBOM[1], S. V. JEFFERS[10], E. GUINAN[11], AND I. RIBAS[12]
[1] Harvard-Smithsonian Center for Astrophysics, Cambridge, MA 02138, USA; jdonascimento@cfa.harvard.edu
[2] Univ. Federal do Rio G. do Norte, UFRN, Dep. de Física, CP 1641, 59072-970, Natal, RN, Brazil
[3] Observatoire de Genève, 51 ch. des Maillettes, CH-1290, Switzerland
[4] Univ. de Toulouse, UPS-OMP, Inst. de R. en Astrop. et Planétologie, France
[5] CNRS, IRAP, 14 Av. E. Belin, F-31400 Toulouse, France
[6] Univ. Grenoble Alpes, IPAG, F-38000 Grenoble, France
[7] Computational Engineering and Science Research Centre, University of Southern Queensland, Toowoomba, 4350, Australia
[8] LUPM-UMR5299, U. Montpellier, Montpellier, F-34095, France
[9] Obs. do Valongo, UFRJ, L. do Pedro Antonio, 43 20080-090, RJ, Brazil
[10] I. für Astrophysik, G.-August-Univ., D-37077, Goettingen, Germany
[11] Univ. of Villanova, Astron. Department, Villanova, PA 19085, USA
[12] Institut de Ciències de l'Espai (CSIC-IEEC), Carrer de Can Magrans, s/n, Campus UAB, E-08193 Bellaterra, Spain
[13] School of Physics, Trinity College Dublin, Dublin 2, Ireland
Received 2016 February 1; accepted 2016 February 24; published 2016 March 16

ABSTRACT

We report magnetic field measurements for κ^1 Cet, a proxy of the young Sun when life arose on Earth. We carry out an analysis of the magnetic properties determined from spectropolarimetric observations and reconstruct the large-scale surface magnetic field to derive the magnetic environment, stellar winds, and particle flux permeating the interplanetary medium around κ^1 Cet. Our results show a closer magnetosphere and mass-loss rate of $\dot{M} = 9.7 \times 10^{-13}\,M_\odot$ yr^{-1}, i.e., a factor of 50 times larger than the current solar wind mass-loss rate, resulting in a larger interaction via space weather disturbances between the stellar wind and a hypothetical young-Earth analogue, potentially affecting the planet's habitability. Interaction of the wind from the young Sun with the planetary ancient magnetic field may have affected the young Earth and its life conditions.

Key words: stars: individual (HD 20630, HIP 15457) – stars: magnetic field – stars: winds, outflows

1. INTRODUCTION

Spectropolarimetric observations allow us to reconstruct the magnetic field topology of the stellar photosphere and to quantitatively investigate the interactions between the stellar wind and the surrounding planetary system. Large-scale surface magnetic field measurements of a young Sun proxy from Zeeman Doppler imaging (ZDI) techniques (Semel 1989; Donati et al. 2006) give us crucial information about the early Sun's magnetic activity.

A key factor for understanding the origin and evolution of life on Earth is the evolution of the Sun itself, especially the early evolution of its radiation field, as well as its particle and magnetic properties. The radiation field defines the habitable zone, a region in which orbiting planets could sustain liquid water at their surface (Huang 1960; Kopparapu et al. 2013). The particle and magnetic environment define the type of interactions between the star and the planet. In the case of magnetized planets, such as the Earth, that developed a magnetic field at least four billion years ago (Tarduno et al. 2015), their magnetic fields act as obstacles for the stellar wind, deflecting it and protecting the upper planetary atmospheres and ionospheres against the direct impact of stellar wind plasmas and high-energy particles (Kulikov et al. 2007; Lammer et al. 2007).

Focused on carefully selected and well-studied stellar proxies that represent key stages in the evolution of the Sun, *The Sun in Time* program from Dorren & Guinan (1994) and Ribas et al. (2005) studied a small sample in the X-ray, EUV, and FUV domains. However, nothing, or little, has been done in this program with respect to the magnetic field properties for those stars. Young solar analogue stars rotate faster than the Sun and show a much higher level of magnetic activity with highly energetic flares. This behavior is driven by the dynamo mechanism, which operates in rather different regimes in these young objects. A characterization of a genuine young Sun's proxy is a difficult task, because ages for field stars, particularly for those on the bottom of the main sequence are notoriously difficult to derive (e.g., do Nascimento et al. 2014). Fortunately, stellar rotation rates for young low-mass stars decrease with time as they lose angular momenta. These rotation rates give a relation to determine stellar age (Kawaler 1989; Barnes 2007; Meibom et al. 2015).

Among the solar proxies studied by the Sun in time, κ^1 Cet (HD 20630, HIP 15457), a nearby G5 dwarf star with $V = 4.85$ and age from 0.4 to 0.6 Gyr (Ribas et al. 2010), stands out as potentially having a mass very close to solar and an age equivilant to that of the Sun when the window favorable to the origin of life opened on Earth around 3.8 Gyr ago or earlier (Mojzsis et al. 1996). This corresponds to the period when favorable physicochemical and geological conditions became established and after the late heavy bombardment. Similar to the Sun at this stage, κ^1 Cet's radiation environment determined the properties and chemical composition of the close planetary atmospheres and provided an important constraint on the role played by the Earth's magnetospheric protection during the critical time at the start of the Archean epoch (Mojzsis et al. 1996) when life is thought to have originated on Earth. This is also the epoch when Mars lost its liquid water inventory at the end of the Noachian epoch some 3.7 Gyr ago (Jakosky & Phillips 2001). A study based on κ^1 Cet can also clarify the biological implications of the high-energy particles at this period (Cnossen et al. 2007). Such a study requires careful analysis based on reasonably bright stars at this specific evolutionary state, and there are only a few bright solar analogues at this age of κ^1 Cet. Stars like Pi[1] UMa and EK Dra are bright enough, but much younger. ϵ Eri is closer to the κ^1 Cet age, but definitely less massive than the Sun.

In this Letter, we investigate the magnetic and particle environments surrounding κ^1 Cet. We also carry out a comprehensive analysis of κ^1 Cet magnetic properties, evolutionary state, rotation, and age. Our goal is to contribute to the understanding of the early Sun's magnetism at a critical time when life arose on Earth and investigate how the wind of a young Sun might have affected the young Earth.

2. OBSERVATIONS AND MEASUREMENTS

Spectropolarimetric data of κ^1 Cet were collected with the NARVAL spectropolarimeter (Aurière 2003) at the 2.0 m Bernard Lyot Telescope (TBL) of Pic du Midi Observatory. NARVAL comprises a Cassegrain-mounted achromatic polarimeter and a bench-mounted cross-dispersed echelle spectrograph. In polarimetric mode, NARVAL has a spectral resolution of about 65,000 and covers the whole optical domain in one single exposure, with nearly continuous spectral coverage ranging from 370 to 1000 nm over 40 grating orders. The data reduction is performed through the Libre-ESpRIT package based on ESPRIT (Donati et al. 1997). In the case of κ^1 Cet, Stokes I and V (circularly polarized) spectra were gathered. This set of κ^1 Cet observations were part of TBL's Bcool Large Program (Marsden et al. 2014). The resulting time series is composed of 14 individual observations collected over 53 consecutive nights, between 2012 October 1 and 2012 November 22. The first seven spectra of the time series were secured over 13 consecutive nights, while weather issues forced a sparser temporal coverage for the second half of the data set. The largest temporal gap between October 31 and November 12, during which more than one rotation period was left uncovered (assuming a rotation period of 9.2 days). Considered altogether and in spite of time gaps, this ensemble of data provides a dense phase coverage of κ^1 Cet, with no phase gap larger than about 0.15. Usually for cool active stars, Stokes V spectra do not display any detectable signatures in the individual spectral lines, even with a peak signal-to-noise ratio (S/N) in excess of 1000 (at wavelengths close to 730 nm). In this situation, we take advantage of the fact that, at first order, Stokes V Zeeman signatures of different spectral lines harbor a similar shape and differ only by their amplitude, so that a multiline approach in the form of a cross-correlation technique is able to greatly improve the detectability of tiny polarized signatures. We employ here the Least-Squares-Deconvolution method (LSD, Donati et al. 1997; Kochukhov et al. 2010) using a procedure similar to the one described in Marsden et al. (2014). Our line-list is extracted from the VALD database (Kupka et al. 2000) and is computed for a set of atmospheric parameters (effective temperature and surface gravity) similar to those of κ^1 Cet. From a total of about 8400 spectral lines recorded in NARVAL spectra and listed in our line mask, the final S/N of Stokes V LSD pseudo-profiles is ranging from 16,000 to 28,000, well enough to detect Zeeman signatures at all available observations (Figure 1).

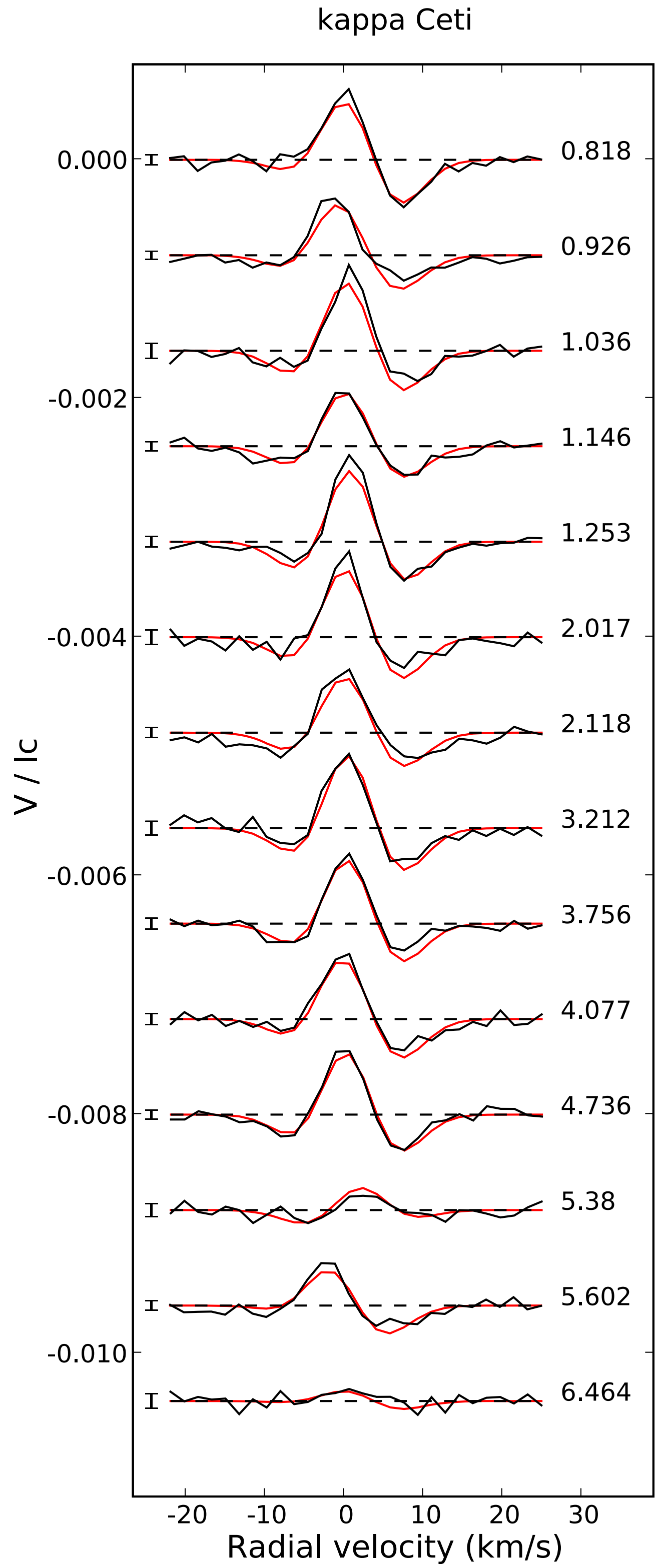

Figure 1. Time series of Stokes V LSD pseudo-profiles. Continuum black lines represent observed profiles and red lines correspond to synthetic profiles of our model. Successive profiles are shifted vertically for display clarity. The rotational cycle is shown on the right of each profile. 1σ error bars for each observation are indicated on the left of each rotational phase (calculated by assuming a rotation period of 9.2 days, and a reference Julian date arbitrary set to 2456195.0). Horizontal dashed lines illustrate the zero levels of each observation.

3. FUNDAMENTAL PARAMETERS AND EVOLUTIONARY STATUS

Based on our NARVAL data, we performed a spectroscopic analysis of κ^1 Cet to redetermine stellar parameters as in do Nascimento et al. (2013) and references therein. We used excitation and ionization equilibrium of a set of 209 Fe I and several Fe II lines and an atmosphere model and mostly laboratory *gf*-values to compute a synthetic spectra. The best solution from this synthetic analysis was fitted to the NARVAL spectrum for the set of parameters $T_{\rm eff} = 5705 \pm 50$ K, [Fe/H] $= +0.10 \pm 0.05$ dex, log $g = 4.49 \pm 0.10$

Several photometric and spectroscopic observational campaigns were carried out to determine κ^1 Cet's fundamental parameters. Ribas et al. (2010) determined the photometric $T_{\rm eff}$ of κ^1 Cet from intermediate-band Strömgren photometry, based on the 2MASS near-IR photometry and a fit of the spectral energy distribution with stellar atmosphere models. This photometric method yielded $T_{\rm eff} = 5685 \pm 45$ K. Ribas et al. (2010) also determined spectroscopic fundamental parameters of κ^1 Cet as $T_{\rm eff} = 5780 \pm 30$ K, log $g = 4.48 \pm 0.10$ dex, and [Fe/H] $= +0.07 \pm 0.04$ dex. Valenti & Fischer (2005) give $T_{\rm eff} = 5742$ K, log $g = 4.49$ dex, and [M/H] $= +0.10$ dex. Paletou et al. (2015), from high-resolution NARVAL Echelle spectra ($R = 65{,}000$, $S/N \sim 1000$) described in Section 2, determined $T_{\rm eff} = 5745 \pm 101$ K, log $g = 4.45 \pm 0.09$ dex, and [Fe/H] $= +0.08 \pm 0.11$. Spectroscopic $T_{\rm eff}$ values are hotter than photometric, and a possible explanation of this offset could be the effects of high chromospheric activity and an enhanced non-local UV radiation field resulting in a photospheric overionization (Ribas et al. 2010). The presented spectroscopic $T_{\rm eff}$ values are in agreement within the uncertainty. Finally, we used our determined solution $T_{\rm eff} = 5705 \pm 50$ K, [Fe/H] $= +0.10 \pm 0.05$ dex, and log $g = 4.49 \pm 0.10$. This yields a logN(Li) = 2.05, in good agreement with Ribas et al. (2010).

To constrain the evolutionary status of κ^1 Cet, we used the spectroscopic solution within computed models with the Toulouse-Geneva stellar evolution code (do Nascimento et al. 2013). We used models with an initial composition from Grevesse & Noels (1993). Transport of chemicals and angular momentum due to rotation-induced mixing are computed as described in Vauclair & Théado (2003). The angular momentum evolution follows the Kawaler (1988) prescription. We calibrated a solar model similar to that of Richard et al. (1996) and used this calibration to compute the κ^1 Cet model. These models, together with the lithium abundance measurement, result in a mass of $1.02 \pm 0.02\,M_\odot$ and an age between 0.5 and 0.9 Gyr for κ^1 Cet, consistent with Güdel et al.'s (1997) estimated age of 0.75 Gyr and Marsden et al.'s (2014) estimated age of 0.82 Gyr using our data and activity-age calibration.

For rotation period $P_{\rm rot}$, such as in do Nascimento et al. (2014), we measured the average surface $P_{\rm rot}$ from light curves. Here we used the *Microvariability and Oscillations of Stars* (*MOST*; Walker et al. 2003) light curve modulation. *MOST* continuously observed κ^1 Cet for weeks at a time providing a $P_{\rm rot}$ (Walker et al. 2003). We extract $P_{\rm rot}$ from the Lomb–Scargle periodogram (Scargle 1982) and a wavelet analysis of the light curve. The $P_{\rm rot}$ obtained was $P_{\rm rot} = 8.77d \pm 0.8$ days, three times lower than the solar $P_{\rm rot}$. The $P_{\rm rot}$ we have measured from the *MOST* light curves allows us an independent (from classical isochrone) age derivation of κ^1 Cet using gyrochronology (Skumanich 1972; Barnes 2007). The gyrochronology age of κ^1 Cet that we derive ranges from 0.4 to 0.6 Gyr, consistent with the predictions from Ribas et al. (2010) and ages determined from evolutionary tracks.

4. THE LARGE-SCALE MAGNETIC FIELD TOPOLOGY

From the time series of Stokes V profiles, we used the ZDI method (ZDI, Semel 1989) to reconstruct the large-scale magnetic topology of the star. Our implementation of the ZDI algorithm is the one detailed by Donati et al. (2006), where the surface magnetic field is projected onto a spherical harmonics frame. We assume during reconstruction a projected rotational velocity equal to 5 km s^{-1} (Valenti & Fischer 2005), a radial velocity equal to 19.1 km s^{-1}, and an inclination angle of 60° (from the projected rotational velocity, radius, and stellar rotation period). We truncate the spherical harmonics expansion to modes with $l \leqslant 10$ since no improvement is noticed in our model if we allow for a more complex field topology. Given the large time span of our observations, some level of variability is expected in the surface magnetic topology. A fair amount of this intrinsic evolution is due to differential rotation, which can be taken into account in our inversion procedure, assuming that the surface shear obeys a simple law of the form $\Omega(l) = \Omega_{\rm eq} - \sin^2(l)d\Omega$, where $\Omega(l)$ is the rotation rate at latitude l, $\Omega_{\rm eq}$ is the rotation rate of the equator, and $d\Omega$ is the difference of rotation rate between the pole and the equator. We optimize the two free parameters $\Omega_{\rm eq}$ and $d\Omega$ by computing a 2D grid of ZDI models spanning a range of values of these two parameters, following the approach of Petit et al. (2002). By doing so, we obtain a minimal reduced χ^2 equal to 1.3 at $\Omega_{\rm eq} = 0.7$ rad days^{-1} and $d\Omega = 0.056$ rad days^{-1}. These values correspond to a surface shear roughly solar in magnitude, with an equatorial rotation period $P_{\rm rot}^{\rm eq} = 8.96$ days, while the polar region rotates in about $P_{\rm rot}^{\rm pole} = 9.74$ days.

Figure 2 from top to bottom presents the inclination of field lines over the stellar surface and the resulting large-scale magnetic geometry. The surface-averaged field strength is equal to 24 G, with a maximum value of 61 G at phase 0.1. The majority (61%) of the magnetic energy is stored in the toroidal field component, showing up as several regions with field lines nearly horizontal and parallel to the equator, e.g., at phase 0.1. The dipolar component of the field contains about 47% of the magnetic energy of the *poloidal* field component, but significant energy is also seen at $\ell > 3$, where 20% of the magnetic energy is reconstructed. Axisymmetric modes display 66% of the total magnetic energy. These magnetic properties are rather typical of other young Sun-like stars previously observed and modeled with similar techniques (Petit et al. 2008; Folsom et al. 2016 and references therein).

5. STELLAR WIND OF κ^1 CET AND ITS EFFECTS ON THE MAGNETOSPHERE OF THE YOUNG EARTH

The spectropolarimetric observations of κ^1 Cet allow us to reconstruct its large-scale surface magnetic field. However, to derive the magnetic environment and particle flux permeating the interplanetary medium around κ^1 Cet, one needs to rely on models of stellar winds. The stellar wind model we use here is identical to the one presented in Vidotto et al. (2012, 2015), in which we use the three-dimensional magnetohydrodynamics (MHD) numerical code BATS-R-US (Tóth et al. 2012) to solve

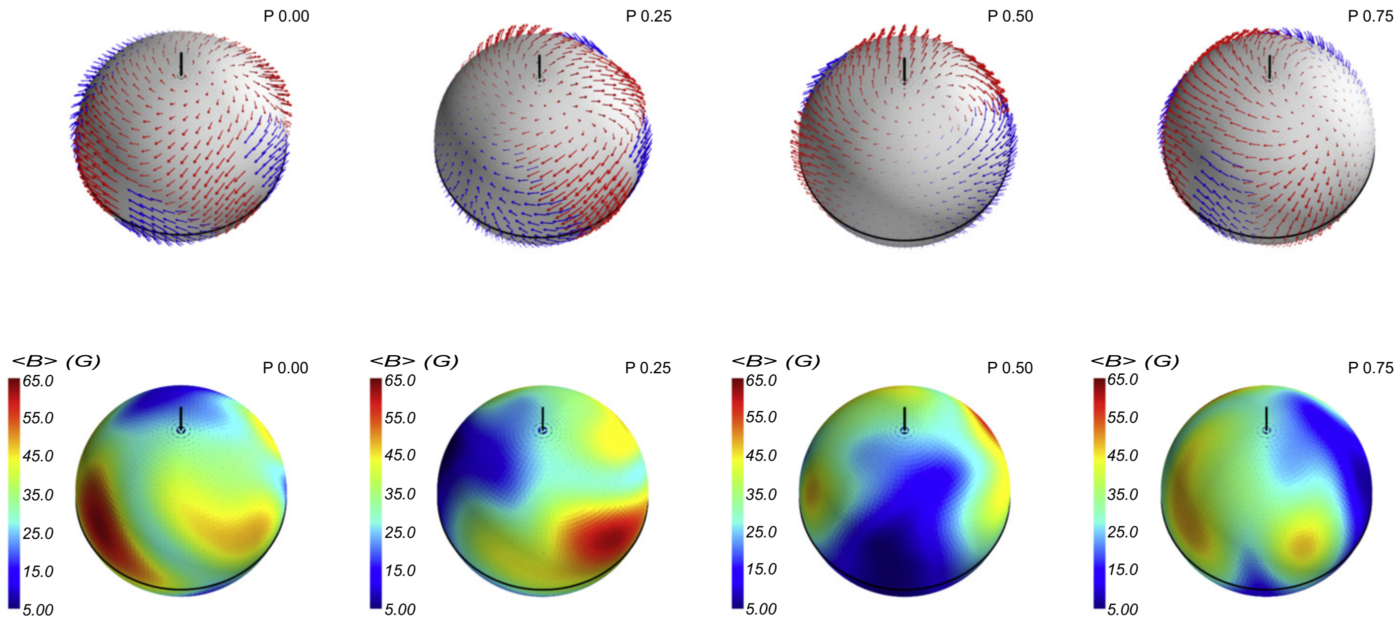

Figure 2. Large-scale magnetic topology of κ^1 Cet at different rotation phases indicated in the top right of each panel. The top row shows the inclination of field lines over stellar surface, with red and blue arrows depicting positive and negative field radial component values, respectively. The bottom row displays the field strength.

the set of ideal MHD equations. In this model, we use, as inner boundary conditions for the stellar magnetic field, the radial component of the reconstructed surface magnetic field of κ^1 Cet (Section 4). We assume that the wind is polytropic, with a polytropic index of $\gamma = 1.1$, and consists of a fully ionized hydrogen plasma. We further assume a stellar wind base density of 10^9 cm^{-3} and a base temperature of 2 MK. Figure 3 shows the large-scale magnetic field embedded in the wind of κ^1 Cet. In our model, we derive a mass-loss rate of $\dot{M} = 9.7 \times 10^{-13} M_\odot$ yr^{-1}, i.e., almost 50 times larger than the current solar wind mass-loss rate. It is interesting to compare our results to the empirical correlation between $\dot{M}$ and X-ray fluxes (F_X) derived by Wood et al. (2014). For κ^1 Cet, the X-ray luminosity is $10^{28.79}$ erg s^{-1} (Wood et al. 2012). Assuming a stellar radius of $0.95\,R_\odot$, we derive $F_X \simeq 10^6$ erg cm^{-2} s^{-1} and, according to Wood et al.'s relation, $\dot{M}$ to be ~63 to 140 times the current solar wind mass-loss rate. Thus, our $\dot{M}$ derivation roughly agrees with the lower envelope of the empirical correlation of Wood et al. (2014) and derived mass-loss rate of Airapetian & Usmanov (2016).

The enhanced mass-loss rate of the young solar analogue κ^1 Cet implies that the strengths of the interactions between the stellar wind and a hypothetical young-Earth analogue is larger than the current interactions between the present-day solar wind and Earth. To quantify this, we calculate the ram pressure of the wind of κ^1 Cet as $P_{\rm ram} = \rho u^2$, where ρ is the particle density and u is the wind velocity (Figure 4). Pressure balance between the magnetic pressure of a hypothetical young-Earth and the ram pressure of the young Sun's wind allows us to estimate the magnetospheric size of the young-Earth:

$$\frac{r_M}{R_\oplus} = f\left(\frac{B_{\rm eq,\oplus}^2}{8\pi P_{\rm ram}}\right)^{1/6}, \qquad (1)$$

where $B_{\rm eq,\oplus}$ is the equatorial field strength of the young Earth dipolar magnetic field and $f \simeq 2^{2/6}$ is a correction factor used

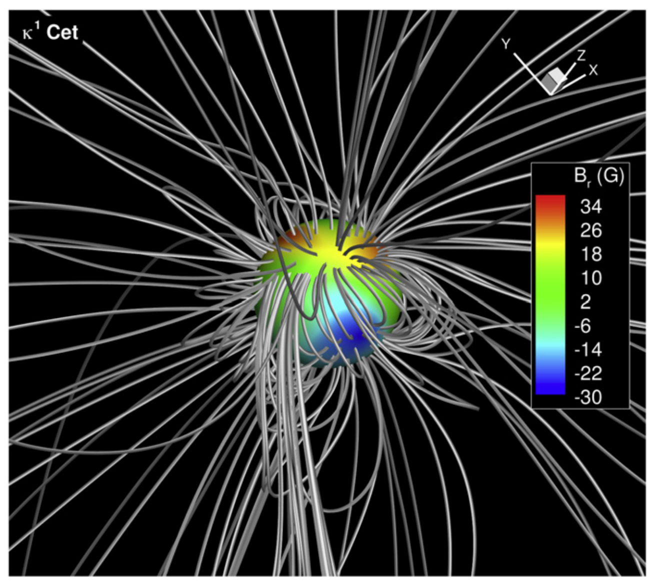

Figure 3. Large-scale magnetic field embedded in the wind of κ^1 Cet. The radial component of the observationally reconstructed surface magnetic field is shown in color.

to account for the effects of currents (e.g., Cravens 2004). Figure 5(a) shows the stand-off distance of the Earth's magnetopause calculated using Equation (1). Here, we assume three values for $B_{\rm eq,\oplus}$: (1) $B_{\rm eq,\oplus} = 0.31$ G, identical to the present-day magnetic field strength (e.g., Bagenal 1992); (2) $B_{\rm eq,\oplus} = 0.15$ G, according to measurements of the Paleoarchean Earth's magnetic field (3.4 Gyr ago; Tarduno et al. 2010); and (3) $B_{\rm eq,\oplus} = 0.40$ G, according to the rotation-dependent dynamo model theory (see Sterenborg et al. 2011). Depending on the assumed field strength of the hypothetical young-Earth, the average magnetospheric sizes are (1) $4.8\,R_\oplus$, (2) $3.8\,R_\oplus$,

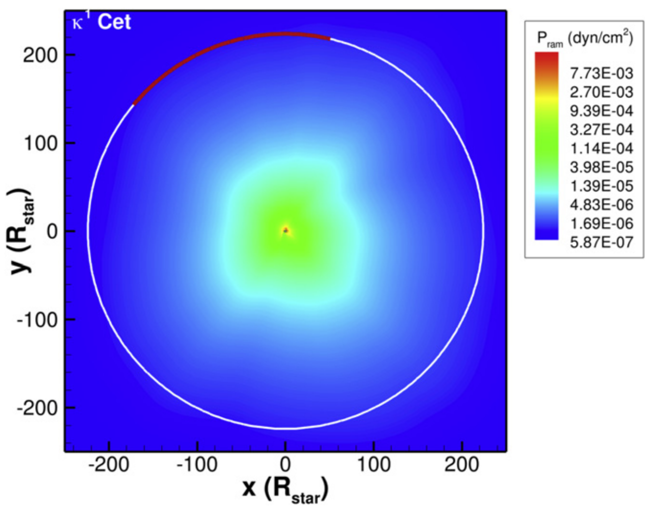

Figure 4. Ram pressure of the stellar wind of κ^1 Cet. The circle indicates the position of the orbit of a young-Earth analogue. Red portions of the orbit indicate regions of the negative vertical component of the interplanetary magnetic field ($B_z < 0$).

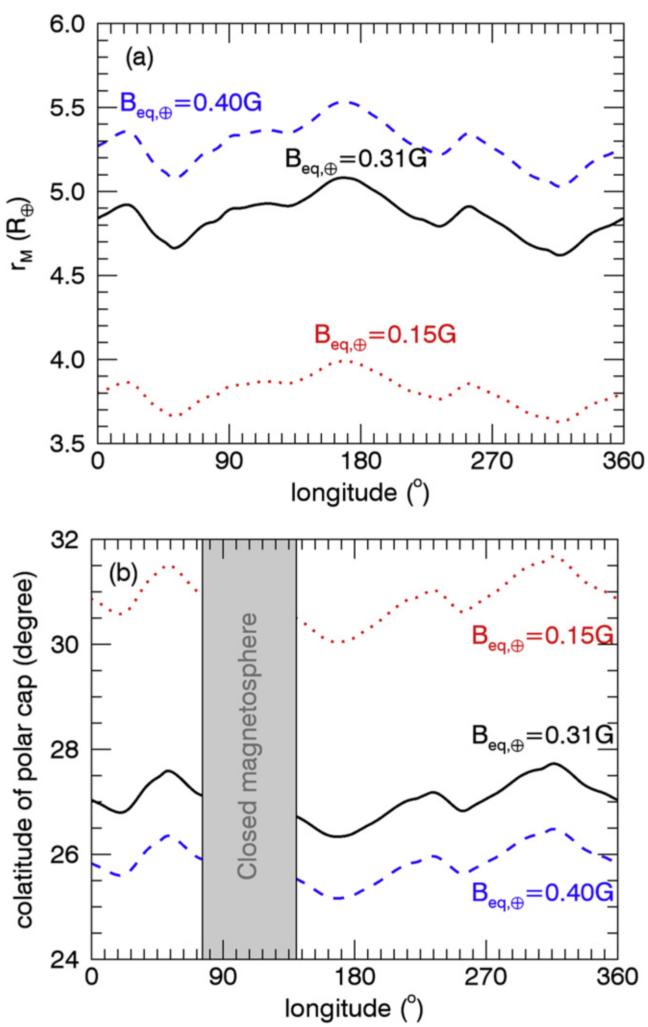

Figure 5. (a) The magnetospheric size of the young-Earth is calculated through pressure balance between the ram pressure of the young Sun's wind (Figure 4) and the magnetic pressure of the planetary magnetosphere (Equation (1)) for different equatorial dipolar field strengths $B_{\mathrm{eq},\oplus}$. (b) The related colatitude of the polar cap, assuming that during most of the orbit, the planetary magnetic moment is parallel to the interplanetary magnetic field.

and (3) 5.3 $R_\oplus$, respectively, indicating a size that is about 34% to 48% the magnetospheric size of the present-day Earth (about 11 $R_\oplus$, Bagenal 1992).

The relative orientation of the interplanetary magnetic field with respect to the orientation of the planetary magnetic moment plays an important role in shaping the open-field-line region (polar cap) of the planet (e.g., Sterenborg et al. 2011). Through the polar cap, particles can be transported to/from the interplanetary space. Tarduno et al. (2010) discusses that the increase in polar cap area should be accompanied by an increase of the volatile losses from the exosphere, which might affect the composition of the planetary atmosphere over long timescales. In the case where the vertical component of interplanetary magnetic field B_z is parallel to the planet's magnetic moment (or anti-parallel to the planetary magnetic field at r_M), the planetary magnetosphere is in its widest open configuration and a polar cap develops. If B_z and the planet's magnetic moment are anti-parallel, there is no significant polar cap.

The complex magnetic-field topology of κ^1 Cet gives rise to non-uniform directions and strengths of B_z along the planetary orbit. The red (white) semi-circle shown in Figure 4 illustrates portions of the orbital path surrounded by negative (positive) B_z. Therefore, depending on the relative orientation between B_z and the planet's magnetic moment, the colatitude of the polar cap will range from 0° (closed magnetosphere) to $\arcsin(R_\oplus/r_M)^{1/2}$ (widest open configuration; e.g., Vidotto et al. 2013). Figure 5(b) shows the colatitude of the polar cap for the case where the planetary magnetic moment points toward positive z. Portions of the orbit where the planet is likely to present a closed magnetosphere (from 76° to 140° in longitude) are blanked out.

6. CONCLUSIONS

We report a magnetic field detection for κ^1 Cet with an average field strength of 24 G, and maximum value of 61 G. The complex magnetic-field topology of κ^1 Cet gives rise to non-uniform directions and strengths along a possible planetary orbit. Our stellar wind model for κ^1 Cet shows a mass-loss rate that is a factor of 50 times larger than the current solar wind mass-loss rate, resulting in a larger interaction between the stellar wind and a hypothetical young-Earth-like planet. With 1.02 $M_\odot$, an age between 0.4 and 0.6 Gyr, κ^1 Cet is a perfect target to study habitability on Earth during the early Sun phase when life arose on Earth. An enhanced mass-loss, high-energy emissions from κ^1 Cet, supporting the extrapolation from Newkirk (1980) and Lammer et al. (2007) of a Sun with stronger activity 3.8 Gyr ago or earlier. Early magnetic fields have affected the young Earth and its life conditions and, due to the ancient magnetic field on Earth four billion years ago as measured by Tarduno et al. (2015), the early magnetic interaction between the stellar wind and the young-Earth planetary magnetic field may well have prevented the volatile losses from the Earth exosphere and create conditions to support life.

The authors wish to thank the *TBL* team. J.D.N. acknowledges CNPq PQ grant and A.A.V. acknowledges the support by the Swiss National Supercomputing Centre (ID s516) and DiRAC (National E-Infrastructure) Data Analytic system at the University of Cambridge, on behalf of the STFC DiRAC HPC Facility funded by ST/K001590/1, STFC (ST/H008861/1, ST/H00887X/1), and STFC DiRAC Operations (ST/K00333X/1). C.P.F was supported by the grant ANR 2011 Blanc SIMI5-6 020 01 Toupies. I.R. acknowledges support from the Spanish Ministry of Economy and Competitiveness (MINECO) and the Fondo Europeo de Desarrollo Regional (FEDER) through grants ESP2013-48391-C4-1-R and ESP2014-57495-C2-2-R.

REFERENCES

Airapetian, V. S., & Usmanov, A. V. 2016, ApJ, 817, 24
Aurière, M. 2003, in EAS Pub. Ser. 9, Magnetism and Activity of the Sun and Stars, ed. J. Arnaud, & N. Meunier (Les Ulis: UDP Sciences), 105
Bagenal, F. 1992, AREPS, 20, 289
Barnes, S. A. 2007, ApJ, 669, 1167
Cnossen, I., Sanz-Forcada, J., Favata, F., et al. 2007, JGRE, 112, 2008
Cravens, T. E. 2004, Physics of Solar System Plasmas (Cambridge: Cambridge Univ. Press)
do Nascimento, J.-D., Jr., García, R. A., et al. 2014, ApJL, 790, L23
do Nascimento, J.-D., Jr., Takeda, Y., et al. 2013, ApJL, 771, L31
Donati, J.-F., Howarth, I. D., Jardine, M. M., et al. 2006, MNRAS, 370, 629
Donati, J.-F., Semel, M., Carter, B. D., et al. 1997, MNRAS, 291, 658
Dorren, J. D., & Guinan, E. F. 1994, in Proc. IAU Colloq. 143, The Sun as a Variable Star, ed. J. M. Pap et al. (Cambridge: Cambridge Univ. Press), 206
Folsom, C. P., Petit, P., Bouvier, J., et al. 2016, MNRAS, 457, 580
Grevesse, N., & Noels, A. 1993, in Origin and Evolution of the Elements, ed. N. Prantzos, E. Vangioni-Flam, & M. Cassé (Cambridge: Cambridge Univ. Press), 15
Güdel, M., Guinan, E. F., & Skinner, S. L. 1997, ApJ, 483, 947
Huang, S.-S. 1960, AmSci, 202, 55
Jakosky, B. M., & Phillips, R. J. 2001, Natur, 412, 237
Kawaler, S. D. 1988, ApJ, 333, 236
Kawaler, S. D. 1989, ApJL, 343, L65
Kochukhov, O., Makaganiuk, V., & Piskunov, N. 2010, A&A, 524, A5
Kopparapu, R. K., Ramirez, R., Kasting, J. F., et al. 2013, ApJ, 765, 131
Kulikov, Y. N., Lammer, H., Lichtenegger, H. I. M., et al. 2007, SSRv, 207, 129
Kupka, F. G., Ryabchikova, T. A., Piskunov, N. E., Stempels, H. C., & Weiss, W. W. 2000, BaltA, 9, 590
Lammer, H., Lichtenegger, H. I. M., Kulikov, Y. N., et al. 2007, AsBio, 7, 185
Marsden, S. C., Petit, P., Morin, J., et al. 2014, MNRAS, 4444, 3517
Meibom, S., Barnes, S. A., Platais, I., et al. 2015, Natur, 517, 589
Mojzsis, S. J., Arrhenius, G., McKeegan, K. D., et al. 1996, Natur, 384, 55
Newkirk, G. 1980, GeCAS, 13, 293
Paletou, F., Böhm, T., Watson, V., & Trouilhet, J.-F. 2015, A&A, 573, A67
Petit, P., Dintrans, B., Solanki, S. K., et al. 2008, MNRAS, 388, 80
Petit, P., Donati, J.-F., & Collier Cameron, A. 2002, ApJ, 771, 31
Ribas, I., Ferreira, L. D., Porto de Mello, G. F., et al. 2010, ApJ, 714, 384
Ribas, I., Guinan, E. F., Gudël, M., & Audard, M. 2005, ApJ, 622, 680
Richard, O., Vauclair, S., Charbonnel, C., et al. 1996, A&A, 312, 1000
Scargle, J. D. 1982, ApJ, 263, 835
Semel, M. 1989, A&A, 225, 456
Skumanich, A. 1972, ApJ, 171, 565
Sterenborg, M. G., Cohen, O., Drake, J. J., & Gombosi, T. I. 2011, JGRA, 116, 1217
Tarduno, J. A., Cottrell, R. D., Davis, W. J., et al. 2015, Sci, 349, 521
Tarduno, J. A., Cottrell, R. D., Watkeys, M. K., et al. 2010, Sci, 327, 1238
Tóth, G., van der Holst, B., Sokolov, I. V., et al. 2012, JCoPh, 231, 870
Valenti, F. A., & Fischer, D. 2005, ApJS, 587, 777
Vauclair, S., & Théado, S. 2003, A&A, 587, 777
Vidotto, A. A., Fares, R., Jardine, M., et al. 2012, MNRAS, 423, 3285
Vidotto, A. A., Fares, R., Jardine, M., et al. 2015, MNRAS, 449, 4117
Vidotto, A. A., Jardine, M., Morin, J., et al. 2013, A&A, 557, A67
Walker, G. A. H., Matthews, J., Kuschnig, R., et al. 2003, PASP, 115, 1023
Wood, B. E., Laming, J. M., & Karovska, M. 2012, ApJ, 753, 76
Wood, B. E., Müller, H.-R., Redfield, S., & Edelman, E. 2014, ApJL, 781, L33